Co-published by
Institute of Fluid-Flow Machinery
Polish Academy of Sciences
Committee on Thermodynamics and Combustion
Polish Academy of Sciences

http://www.imp.gda.pl/archives-of-thermodynamics/

ARCHIVES OF THERMODYNAMICS

Effects of Joule heating due to magnetohydrodynamic slip flow in an inclined channel

Jagadeeshwar Pashikanti[a*], Santhosh Thota[a], Susmitha Priyadharshini[a]

[a]Indian Institute of Information Technology Tiruchirappalli, Trichy - Madurai Highway, Sethurapatti, Tamil Nadu 620012, India
*Corresponding author email: jagadeeshwarp@iiitt.ac.in

Received: 25.07.2023; revised: 12.01.2024; accepted: 05.05.2024

Abstract

Graphene oxide nanoparticles with higher thermal conductivity aid in enhancing the flow and heat transport in magnetohydrodynamic devices such as magnetohydrodynamic pumps. Modelling such devices with promising applications inherently necessitates entropy studies to ensure efficient models. This investigation theoretically studies the entropy generation in magnetohydrodynamic flow of graphene oxide in an inclined channel. Buongiorno nanofluid model is used including the impacts of nanoparticle attributes, namely thermophoretic and Brownian diffusion along with viscous dissipation effects. The spectral quasi-linearization method with Chebyshev's polynomials is adapted to solve the differential equations under slip conditions. On studying the effects of implanted parameters, it is concluded that the conductive heat transfer enhancement by the Hartmann number is remarked. The Bejan number is found to be greater than 0.9 and hence, heat transfer primarily causes the entropy generation. A good agreement is found between the results for special cases and the results from the literature. Furthermore, investigations conclude that entropy is contributed primarily by heat transfer.

Keywords: Graphene nanofluids; Entropy generation; Buongiorno model

Vol. 45(2024), No. 3, 89–98; doi: 10.24425/ather.2024.151219

Cite this manuscript as: Pashikanti, J., Thota, S., & Priyadharshini, S. (2024). Effects of Joule heating due to magnetohydrodynamic slip flow in an inclined channel. *Archives of Thermodynamics*, 45(3), 89–98.

1. Introduction

Nanofluids are preferred to other conventional viscous and microfluids for their effective heat transfer properties. Additionally, they keep the flow channels from obstruction, deposition and erosion. Literature suggests that thermophoresis and Brownian motion affect the sole significant slip mechanisms in nanofluid flows [1]. The performance of nanofluids varies according to the volume fraction, choice of geometry, base fluids and hybridized nanoparticles, and the needs in demand [2–4]. However, the results from computational studies conclude that graphene oxide (GO) aids in maximizing heat transfer rates because of its excellent thermal conductivity [5–8]. Some of the applications of graphene-based nanofluids include their use in lithium-ion batteries, biosensors, supercapacitors, medical suspensions, etc.

Some classical numerical studies on the fluid flow in inclined channels include the study of fully developed laminar flow in the channel of two parallel plates with an inclination angle. The opposing flow was studied under uniform flux conditions with actual flow characteristics [9]. Choi and Eastman [10] studied the impacts of natural convective flow with a heat source between two parallel plates. The results show a strong dependence of the Nusselt number on the inclination angle for values

Nomenclature

B_0 – magnetic field strength
Be – Bejan number, Be = N_{Sh}/N_S
C – concentration, -
C_p – specific heat capacity, J/(kg·K)
C_f – skin friction
D_B – Brownian diffusivity
Ec – Eckert number, Ec = $U_0^2/(\kappa_{bf}C_{pbf}(T_2\text{-}T_1))$
g – gravity, m/s^2
Gr – Grashof number
h – domain height, m
Ha – Hartmann number
J – Joule heating parameter
M_m – parameter of combined mass and heat transfer, $M_m = RD_BC_0/\kappa_{bf}$
N_b – Brownian motion parameter
N_r – Buoyancy ratio
N_s – nondimensional entropy generation number
Nu – Nusselt number
p – pressure, Pa
Pr – Prandtl number, Pr = $\mu C_{pbf}/\kappa_{bf}$
Re – Reynolds number
R_{SC} – suction/injection parameter
S – slip parameter
S_G – entropy generation rate
Sh – Sherwood number
S_u – velocity slip length/factor, m
T – temperature, K
u – velocity, m/s
v_0 – suction/injection velocity
x, y – Cartesian coordinates, m

Greek symbols

α – inclination angle, rad
β – thermal expansion coefficient, 1/K
κ – thermal conductivity, W/(m K)
μ – dynamic viscosity, Pa s
ρ – density, kg/m^3
σ – electrical conductivity
τ – heat capacity ratio
Ω_T – temperature parameter, $\Omega_T = T_2/T_1$

Subscripts and Superscripts

a – upper plate
b – lower plate
bf – base fluid
nf – nanofluid
sp – solid particle
S_G – irreversibilities caused by combined heat and mass transfer
S_h – irreversibilities caused by heat transfer and fluid friction

Abbreviations and Acronyms

GO – graphene oxide
MHD – magnetohydrodynamics
ODE – ordinary differential equation
PHP – pulsating heat pipe
SLM – successive linearization method

higher than π/4. Talabi and Nwabuko [11] numerically analysed the convective heat transfer flow in an inclined channel comprising a parabolic and a horizontal wall under isothermal and constant heat flux conditions. Solutions using the staggered differencing (SD) technique suggest that Grashof and Prandtl numbers improve the Nusselt number for both isothermal and heat flux cases.

Literature suggests that GO and hybrid graphene nanoparticles suspended in ethylene glycol (EG) and water (H_2O) are the common graphene-based nanofluids in theoretical and experimental studies [12]. Analytical investigations on GO nanofluid flow in moving plates suggest a significant improvement in heat transfer with improved nanoparticle volume fractions [13]. Gul et al. [14] conducted a comparative analysis of GO flow dispersed in water and ethylene glycol (W-EG) in an upright channel with interpretations that the ethylene glycol (EG) based nanofluid has a higher thermal efficiency than water. Shahzad et al. [15] analysed the experimental and theoretical impacts of kerosene-based GO nanofluid flow on a parabolic trough surface accumulator (PTSC). A 15% enhancement in heat transfer rate of the nanofluid in comparison to kerosene is documented. Nazari et al. [16] experimented to study the impacts of varying concentrations of W-GO nanofluids on pulsating heat pipe (PHP). From the results, it is interpreted that the nanoparticles positively impacted the heat transfer of water in lower concentrations. The impacts were negative for a high concentration of 1.5 grams per litre. Dehghan et al. [17] analysed the effects of forced convective flow of GO nanofluids in an inclined backwards-facing step (BFS). Simulations of the microchannel of double BFS show a 12.3% enhancement in heat transfer coefficient compared to that of water. Pashikanti et al. [18] conducted an entropy generation analysis on the flow of graphene oxide nanofluid in an inclined channel in the presence of a magnetic field. They concluded that the flow velocity enhancement by the Hartmann number is remarked.

Graphene-based nanofluids yield amplified industrial significance when hybridised with other metal or semi-conductor nanoparticles and polymers. For instance, they are used in adsorbent materials, lubricant additives, humidity sensors, photocatalysis and heat transfer applications. Javanmard et al. [19] investigated the magnetohydrodynamic (MHD) flow of W-GO nanofluids in a horizontal channel due to forced convection. Numerical results are interpreted to enhance the convection at the walls with nanoparticle volume fraction.

Hafeez et al. [20] numerically analysed the Jeffery-Hamel flow of copper and GO nanoparticles in convergent and divergent channels. The magnetic parameter is seen to lower the skin friction drag in the magnetohydrodynamic flow. Raza et al. [21] investigated the impacts of the convective flow of Casson fluid dispersed with GO and molybdenum disulphide (MoS_2) nanoparticles. A fractional derivative model is developed, and the results show that the Atangana-Baleanu (AB) model is stable compared to the Caputo-Fabrizio (CF) model, and the velocity profiles decrease with the fractional parameters. Computational fluid flow investigations on hybrid graphene nanofluids, such as the study of the impacts of shape factors due to the flow of kerosene-based GO and MoS_2 nanofluids in an inclined porous channel, reveal the enhancement of heat transfer with laminashaped nanoparticles [22].

Combining the magnetohydrodynamic studies with nanofluidics is essential for their applications in industries and biomedicine, such as molten pumps contributing to coolants in nuclear reactors, drug delivery, etc. Similarly, studying the impacts of viscous dissipation on fluid flow helps with a better understanding of the energy loss due to the interactions of liquid particles, thereby aiding the utilisation of the fluids as better lubricants. Akram et al. [23] studied the flow of Oldroyd 4-constant nanofluids in a non-uniform inclined channel with magnetic field and cross-diffusion effects. From the results obtained, chemical reaction and Brownian motion are interpreted to reduce mass transfer. Nazeer [24] analysed Eyring-Powell fluid flow suspended with gold and silver particles, including magnetic field effects. The results document a lesser skin friction drag for gold particles than for silver particles. Yasin et al. [25] analysed the impacts of an inclined magnetic field on the flow of blood-based nanofluid hybridised with silver and copper nanoparticles in a symmetric channel. Studying the effects of Joule heating, viscous dissipation, heat sink/source and thermal radiation, the conclusions reveal that the magnetic effects positively affect velocity while reducing the temperature, and the homogeneous reactions are found to improve blood circulation.

Computational fluid flow studies under convective conditions, such as the analysis of entropy in an inclined channel due to micropolar fluid flow under convective and slip conditions by Srinivasacharya and Hima Bindu reveal that the Reynolds number and coupling number keep the entropy in check [26]. The interesting works on steady Maxwell fluid past an exponentially stretching/shrinking sheet with various effects along multiple slip conditions show that the values of the skin friction, Nusselt number and Sherwood number decline due to enhancement in the time relaxation parameter; temperature and concentration distribution decline due to thermal and concentration stratification parameters and incline due to the relaxation parameter, and the mass transfer rate augments due to the thermophoretic parameter [27–29]. Further studies on micropolar fluids over exponentially stretching cylinders under slip conditions with microorganisms reveal that skin friction declines. At the same time, the Nusselt number inclines with stretching and micropolar parameters; velocity, thermal energy, and microorganism numbers enhances by the slip parameter, while temperature increases with the time relaxation parameter. A transient two-dimensional radiative Oldroyd-B nanofluid flow is examined by e.g. Khan, Nadeem and Ahmad et al. [30−34] on an exponentially stretching porous surface with microorganisms to improve the stability of the nanofluid. The results reveal that the higher values of the relaxation parameter correspond to the maximum heat and mass transfer rate.

The contribution of graphene-based nanoparticles to renewable energy and thermal conductivity enhancement reassures economically large-scale applications as coolants and in power storage and capacity. Hence, computationally investigating graphene-based nanofluids flow in several geometries is significant for qualitative references. The novelty of this paper is that it aims to bridge the gap of computationally studying the impacts of Joule heating due to the flow of GO nanoparticles dispersed in water in an inclined channel, which is an unexplored problem. The flow is modelled, and the equations are numerically solved to graph the results.

2. Mathematical formulation

The flow geometry comprises two parallel plates aligned with an angle of inclination α (in radians). Water with dispersed GO nanoparticles flows steadily in the channel. The representative flow picture is shown in Fig. 1.

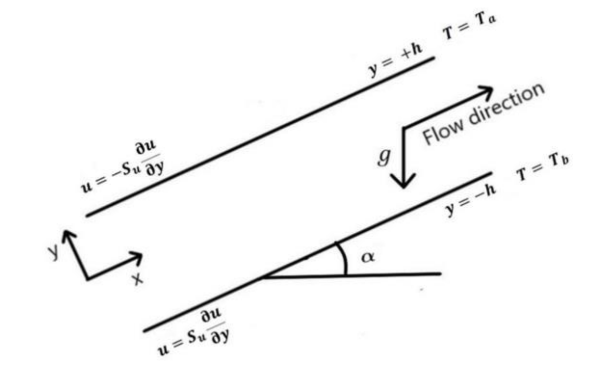

Fig. 1. Representative picture of the problem.

We consider the body forces due to gravity and the characteristic effects such as Brownian motion and thermophoresis, which are the only significant slip mechanisms in nanofluid flows. Irrespective of the flow, Brownian motion is the random motion of nanoparticles in the fluid, and thermophoresis is the movement of the nanoparticles from hotter to colder regions. Thus, the problem is modelled, taking into account the aforementioned effects and adapting the Buongiorno nanofluid model [1] as follows:

$$\frac{\partial u}{\partial x} = 0, \tag{1}$$

$$\rho_{nf} v_0 \frac{\partial u}{\partial y} + \frac{\partial p}{\partial x} = \mu_{nf} \frac{\partial^2 u}{\partial y^2} + \Big((\rho\beta)_{nf} (T - T_a)(1 - C_a) + -(\rho_{sp} - \rho_{bf})(C - C_a) \Big) g \sin\alpha - \sigma_{nf} B_0^2 u, \tag{2}$$

$$\frac{\kappa_{nf}}{(\rho C_p)_{nf}} \left(\frac{\partial^2 T}{\partial y^2}\right) + \tau D_B \frac{\partial C}{\partial y} + \tau \frac{DT}{T_a} \left(\frac{\partial T}{\partial y}\right)^2 + \frac{\sigma_{nf}}{(\rho c p)_{nf}} B_0^2 u^2 = 0 \tag{3}$$

$$D_B \frac{\partial^2 C}{\partial y^2} + \frac{DT}{T_a} \frac{\partial^2 T}{\partial y^2} = 0, \tag{4}$$

and the slip boundary conditions are

– at $y = -h$: $\quad u = S_u \frac{\partial u}{\partial y}, \quad T = T_a, \quad C = C_a,$ (5a)

– at $y = h$: $\quad u = -S_u \frac{\partial u}{\partial y}, \quad T = T_b, \quad C = C_b.$ (5b)

The notations T_a, T_b, C_a and C_b represent fluid temperatures (in Kelvin) and concentrations at the upper and lower plates, respectively and S_u is the velocity slip length/factor (in meter) which reflects the amount of liquid slip at a given surface. The slip length is the distance beyond the solid–liquid interface where the liquid velocity linearly extrapolates to zero.

Table 1 presents the values of thermophysical properties [35,36], and their definitions are as follows:

$$\mu_{nf} = \frac{\mu_{bf}}{(1-\Phi)^{2.5}}, \tag{6a}$$

$$\rho_{nf} = (1-\Phi)\rho_{bf} + \Phi\rho_{sp}, \tag{6b}$$

$$(\rho C_p)_{nf} = (1-\Phi)(\rho C_p)_{bf} + \Phi(\rho C_p)_{sp}, \tag{6c}$$

$$(\rho\beta)_{nf} = (1-\Phi)(\rho\beta)_{bf} + \Phi(\rho\beta)_{sp}, \tag{6d}$$

$$\frac{\kappa_{nf}}{\kappa_{bf}} = \frac{\kappa_{sp}+2\kappa_{bf}+2\Phi(\kappa_{bf}-\kappa_{sp})}{\kappa_{sp}+2\kappa_{bf}-\Phi(\kappa_{bf}-\kappa_{sp})}, \tag{6e}$$

$$\alpha_{nf} = \frac{\kappa_{nf}}{(\rho C_p)_{nf}}. \tag{6f}$$

The subscripts *nf*, *sp* and *bf* indicate nanofluid, solid particle and base fluid. In contrast, the quantities κ, C_p, β, μ and ρ, respectively, denote thermal conductivity, specific heat capacity, thermal expansion coefficient, dynamic viscosity and density.

Table 1. Thermophysical properties [37–40].

Property and units	Water	GO
ρ, kg/m³	997.1	1800
C_p, J/(kg K)	4179	717
κ, W/(m K)	0.613	5000
β, 10^{-5}/K	21	28.4
σ, S/m	0.005	10^7

The following similarity variables are used to transform the modelled equations Eqs. (1)–(5):

$$\eta = \frac{y}{h}, \quad u = U_0 f(\eta), \quad \theta = \frac{T-T_a}{T_b-T_a}, \quad \varphi = \frac{C-C_a}{C_b-C_a}. \tag{7}$$

The transformed ODEs are given as:

$$f'' - A_1 R_{SC} f' + \frac{\mathrm{Gr}}{\mathrm{Re}} A_2 (A_3\theta - N_r\phi)\sin\alpha - A_2 P_1 - A_4 \mathrm{Ha} f = 0, \tag{8}$$

$$\theta'' + A_5(N_b\theta'' + N_t\phi'^2) + A_6 J f^2 = 0, \tag{9}$$

$$\phi'' + \frac{N_t}{N_b}\theta'' = 0, \tag{10}$$

such that

– at $\eta = -1$: $\quad f - S f' = 0, \quad \theta = 0, \quad \phi = 0,$ (11a)

– at $\eta = 1$: $\quad f + S f' = 0, \quad \theta = 1, \quad \phi = 1.$ (11b)

The constant coefficients (A_i, I = 1 to 6) and the dimensionless parameters used namely the suction/injection parameter R_{SC}, the buoyancy ratio N_r, heat capacity ratio τ, thermophoresis parameter N_t, Brownian motion parameter N_b, Grashof number Gr, Reynolds number Re, Hartmann number Ha, Joule heating parameter J and slip parameter S are defined as:

$$A_1 = 1 - \Phi + \Phi\frac{\rho_{sp}}{\rho_{bf}}, \qquad A_2 = (1-\Phi)^{2.5},$$

$$A_3 = 1 - \Phi + \frac{\Phi(\rho\beta)_{sp}}{(\rho\beta)_{bf}}, \qquad A_4 = \frac{\sigma_{nf}}{\sigma_{bf}}(1-\Phi)^{2.5},$$

$$A_5 = 1 - \Phi + \frac{\Phi(\rho C_p)_{sp}}{(\rho C_p)_{bf}}, \qquad A_6 = \frac{\sigma_{nf}\kappa_{bf}}{\sigma_{bf}\kappa_{nf}},$$

$$\mathrm{Pr} = \frac{\mu_{bf}C_{pbf}}{\kappa_{bf}}, \qquad \mathrm{Ha} = \frac{\sigma_{bf}B_0^2h^2}{\mu_{bf}}, \qquad J = \frac{\sigma_{bf}B_0^2U_0^2h^2}{\kappa_{bf}(T_b-T_a)},$$

$$R_{sc} = \frac{\rho_{bf}}{\mu_{bf}}v_0 h, \qquad \mathrm{Gr} = \frac{g\beta_{bf}(1-C_a)(T_b-T_a)h^3\rho_{bf}^2}{\mu_{bf}^2},$$

$$N_r = \frac{(\rho_{sp}-\rho_{bf})(C_b-C_a)}{(\rho\beta)_{bf}(T_b-T_a)(1-C_a)}, \qquad N_t = \frac{\tau D_T(T_b-T_a)}{\alpha_{bf}T_a}, \qquad S = \frac{S_u}{d},$$

$$P_1 = \frac{h^2}{v_0\mu_{bf}}\frac{\partial p}{\partial x}, \qquad \mathrm{Re} = \frac{\rho_{bf}U_0 h}{\mu_{bf}}, \qquad N_b = \frac{\tau D_B(C_b-C_a)}{\alpha_{bf}}.$$

Practically significant values such as Sherwood number Sh, skin friction C_f and Nusselt number Nu are derived as:

– at $\eta = \pm 1$

$$\mathrm{Nu} = -\theta'(\eta), \quad \mathrm{Sh} = -\phi'(\eta), \quad C_f = c_1 f'(\eta),$$

where the constant c_1 is given by:

$$c_1 = (1-\Phi)^{-2.5}\left((1-\Phi) + \Phi(\rho_{sp}/\rho_{bf})\right)^{-1}.$$

In the next section, a derivation and an analysis for the entropy is presented.

3. Entropy analysis

The entropy generation analysis is done in order to understand and minimize the loss of energy and thereby enhancing the efficiency of the model and performance of the device. By the law of increased entropy, the generated entropy is contributed from temperature, viscous dissipation and concentration. Thus, the entropy generation rate, S_G is written as [41]:

$$S_G = \frac{\kappa_{nf}}{T_a^2}\left(\frac{\partial T}{\partial y}\right)^2 + \frac{\mu_{nf}}{T_a}\left(\frac{\partial u}{\partial y}\right)^2 + RD_b\left(\frac{1}{C_a}\left(\frac{\partial C}{\partial y}\right)^2 + \frac{1}{T_a}\left(\frac{\partial T}{\partial y}\right)\left(\frac{\partial C}{\partial y}\right)\right) + \frac{\sigma_{nf}B_0^2}{T_a}u^2. \tag{12}$$

Here, the expressions on the right side are ascribed to the thermodynamic irreversibilities caused by temperature, fluid friction and combined mass and heat transfer. From S_G and characteristic entropy generation rate, $S_{G0} = \kappa_{nf}(T_2-T_1)^2/(T_1L)^2$, we write the nondimensional entropy generation number as $N_S = S_G/S_{G0}$.

From Eqs. (7) and (12), we have:

$$\frac{\eta^2}{4}N_s = \frac{1}{\chi}\left(\theta'^2 + c_2\frac{\mathrm{EcPr}}{\Omega_T}f'^2 + c_3M_m\frac{\Omega_C}{\Omega_T}\left(\frac{\Omega_C}{\Omega_T}\phi' + \theta'\right) + c_4\frac{J}{\Omega_T}f^2\right) = N_{S_h} + N_{S_G} + N_{S_J}, \tag{13}$$

where the subscripts S_h, S_G and S_J respectively correspond to the irreversibilities caused by heat transfer and fluid friction, combined heat and mass transfer and Joule heating. The parameters in Eq. (13) are given by constant $\chi = h^2/L^2$, temperature parameter $\Omega_T = T_2/T_1$, concentration parameter $\Omega_C = C_2/C_1$, and the parameter of combined mass and heat transfer $M_m = RD_BC_0/\kappa_{bf}$, Eckert number $\mathrm{Ec} = U_0^2/(\kappa_{bf}C_{pbf}(T_2-T_1))$, Prandtl number $\mathrm{Pr} = \mu C_{pbf}/\kappa_{bf}$ and the constants are given by $c_2 = (1-\Phi)^{-2.5}\kappa_{bf}/\kappa_{nf}$ and $c_3 = (1-\Phi)^{2.5}$, $c_4 = (\kappa_{bf}\sigma_{nf})/(\kappa_{nf}\sigma_{bf})$.

Bejan number, $\mathrm{Be} = N_{Sh}/N_S$ determines the principal source for entropy generation [42]. From this ratio, it is dictated that heat transfer mainly influences the entropy if Be > 0.5, while, fluid friction and mass and heat transfer fundamentally contributes to the entropy if Be < 0.5 and all the three irreversibilities contribute equally if Be = 0.5 [43].

4. Numerical solution

The ODEs (8)–(11) are solved by adapting the spectral quasilinearization method (SQLM) [26,44,45] and the solution procedure is as follows:

i. The nonlinear terms about the solution are expanded using the Taylor series, and the higher-order derivatives are neglected.
ii. The spectral collocation method is applied to the linearised equations, and the functions are iterated using Chebyshev polynomials at the collocation points.
iii. A suitable bijection is mapped from the domain to the collocation points.
iv. Approximations and the derivatives are substituted in the linearized equations to obtain a matrix equation, which is solved using MATLAB.

We linearize the nonlinear terms by using the expansion of Taylor series. Let f_r, θ_r and ϕ_r be the solution of the differential equations. Then, assuming f_{r+1}, θ_{r+1} and ϕ_{r+1} to be the improved solutions, the system of ODEs is solved using an iterative method. By expanding the nonlinear terms using the expansion of Taylor series about the solution and discarding the higher derivatives, the following linearized equations and their associated boundary conditions are obtained:

$$f''_{r+1} + a_{1,r}f'_{r+1} + a_{2,r}f_{r+1} + a_{3,r}\theta_{r+1} + a_{4,r}\phi_{r+1} = a_{5,r}, \quad (14)$$

$$b_{1,r}f_r + \theta''_{r+1} + b_{2,r}\theta'_r + b_{3,r}\phi_r = b_{4,r}, \quad (15)$$

$$c_{1,r}\theta''_{r+1} + \phi''_{r+1} = 0, \quad (16)$$

such that

– at $\eta = -1$: $f_{r+1} - S\,f'_{r+1} = 0, \quad \theta_{r+1} = \phi_{r+1} = 0,$ (17a)

– at $\eta = 1$: $f_{r+1} + S\,f'_{r+1} = 0, \quad \theta_{r+1} = \phi_{r+1} = 1.$ (17b)

The coefficients in the above equations are given by:

$$a_{1,r} = -A_1R_{sc}, \quad a_{2,r} = -A_4\mathrm{Ha}, \quad a_{3,r} = A_2A_3\frac{\mathrm{Gr}}{\mathrm{Re}}\sin\alpha,$$

$$a_{4,r} = -A_2\frac{\mathrm{Gr}}{\mathrm{Re}}\mathrm{Nr}\sin\alpha, \quad a_{5,r} = A_2P_1, \quad b_{1,r} = 2A_6J\,f_r,$$

$$b_{2,r} = A_5N_b\phi'_r + 2A_5N_t\phi'_r, \; b_{3,r} = A_5N_b\theta'_r,$$

$$b_{4,r} = A_5N_b\theta'_r\phi'_r + A_5N_t\theta'^2_r + A_6J\,f_r^2, \qquad c_{1,r} = \frac{N_t}{N_b}.$$

We apply the collocation method by using Chebyshev polynomials and iterating f, θ and ϕ at the Gauss-Lobatto collocation points $\xi_j = \cos(\pi j/N)$, $j = 0, 1, 2, ..., N$ [45]. Thus, we approximate the unknown functions as:

$$f_{r+1}(\xi) = \sum_{k=0}^{N} f_{r+1}(\xi_k)T_k(\xi_j),$$
$$\theta_{r+1}(\xi) = \sum_{k=0}^{N} \theta_{r+1}(\xi_k)T_k(\xi_j), \quad (18)$$
$$\phi_{r+1}(\xi) = \sum_{k=0}^{N} \phi_{r+1}(\xi_k)T_k(\xi_j),$$

where Chebyshev polynomial $T_k(\xi)$ is given by:

$$T_k(\xi) = \cos(k\cos^{-1}(\xi)).$$

Further, the following equations give the derivatives:

$$\frac{d^r f_{r+1}}{d\,\eta^r} = \sum_{k=0}^{N} D_{kj}^r f_{r+1}(\xi_k), \qquad j = 0, 1, ..., N,$$
$$\frac{d^r \theta_{r+1}}{d\,\eta^r} = \sum_{k=0}^{N} D_{kj}^r \theta_{r+1}(\xi_k), \qquad j = 0, 1, ..., N, \quad (19)$$
$$\frac{d^r \phi_{r+1}}{d\,\eta^r} = \sum_{k=0}^{N} D_{kj}^r \phi_{r+1}(\xi_k), \qquad j = 0, 1, ..., N.$$

Here $\mathcal{D} = D/2$ is called the Chebyshev differentiation matrix.

On substituting Eq. (18) and Eq. (19) in Eqs. (14)–(17), we obtain:

$$AY_{r+1} = R_r, \quad (20)$$

associated with the conditions:

$$(1 + SD_{00})f_{r+1}(\xi_0) + S\sum_{k=1}^{N} D_{0k}f_{r+1}(\xi_k) = 0, \quad (21a)$$

$$\theta_{r+1}(\xi_0) = \phi_{r+1}(\xi_0) = 0, \quad (21b)$$

$$-S\sum_{k=0}^{N-1} D_{Nk}f_{r+1}(\xi_k) + (1 - SD_{NN})f_{r+1}(\xi_N) = 0, \quad (21c)$$

$$\theta_{r+1}(\xi_N) = \phi_{r+1}(\xi_N) = 1. \quad (21d)$$

We choose the initial approximations $f_0 = 0$, $\theta_0 = \phi_0 = (1-\eta)/2$ in order to satisfy Eq. (17) and the Eq. (20) is recursively iterated at ξ_j, $j = 0, 1, ..., N$ by substituting Eq. (21), to the order of approximation. Hence, the obtained solution is graphed and interpreted. These initial conditions are iterated to obtain the numerical solution.

5. Results

The equation (20) is solved to graphically depict the results with interpretations. The parameters are varied in the practical range and the effects of different parameters are studied [46,47]. Since, the Newtonian behavior of water based nanofluid is considered, fixed values of $\Phi = 0.01$ and $\mathrm{Pr} = 6.5$ are taken. The other parameter values are taken to be as $\mathrm{Ec} = 10^{-5}$, $\mathrm{Gr} = 2\times10^5$, $S = 0.5$, $N_b = 4\times10^{-4}$, $\mathrm{Re} = 300$, $N_t = 2\times10^{-4}$, $R_{sc} = 5$, $\alpha = \pi/4$, $J = 3\times10^{-5}$, $\mathrm{Ha} = 2$ and $N_r = 2$, unless mentioned otherwise. The order of SLM approximation is taken to be $N = 100$ and the convergence of results is obtained at a tenth iteration. The results for the case

Table 2. Comparison of $f(\eta)$ calculated by the present method for Ec = R_{SC} = 1, P_1 = -1, Pr = 0.71 and S = J = Ha = 0 and A_i = 1, (i = 1, 2, 3, 4, 5, 6) [48] (an approximation of η values is taken, because of the use of Gauss-Lobatto collocation points).

Present study		Makinde and Eegunjobi [48]	
η	$f(\eta)$	η	$f(\eta)$
0	0	0	0
0.100158	0.038849	0.1	0.038793
0.201048	0.071451	0.2	0.071149
0.299985	0.096387	0.3	0.09639
0.400145	0.113789	0.4	0.113769
0.500000	0.122459	0.5	0.122459
0.601394	0.121461	0.6	0.121546
0.700015	0.110017	0.7	0.11002
0.80021	0.086702	0.8	0.086764
0.900783	0.050207	0.9	0.050545
1	0	1	0

of Ec = R_{sc} = 1, P_1 = −1, Pr = 0.71 and S = J = Ha = 0 agree with the results from Makinde and Eegunjobi [48] (refer to Table 2). Figure 2 depicts the influence of Re on f, N_S and Be. With the rising Reynolds number, viscous forces decrease and the nanofluid moves with a greater velocity. Hence, the flow velocity increases in the proximity of the upper plate and a lesser velocity is observed near the lower plate (Fig. 2a). Similarly, entropy number decreases near the upper plate and increases near the lower plate (Fig. 2b). There is a consequent increase in Bejan number, suggesting the contribution of mass transfer and fluid friction and to the generated entropy (Fig. 2c).

The impacts of α on f, N_S and Be are presented in Fig. 3. As the angle of inclination increases, a drop in velocity is observed (Fig. 3a). Whereas, an increase in angle of inclination values causes an enhancement in N_S values (Fig. 3b). This consequently causes the Bejan number to decrease (Fig. 3c), thus pronouncing the contribution of fluid friction and mass transfer to the generated entropy.

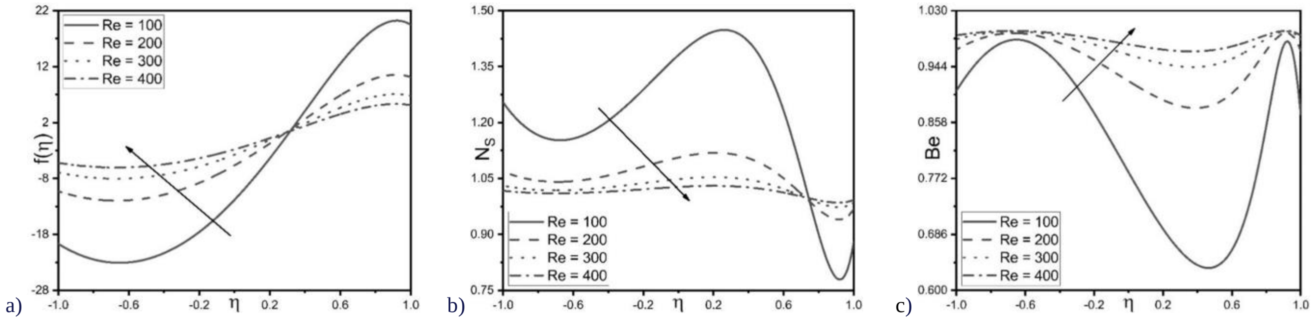

Fig. 2. Impacts of Re on:(a) f, b) N_S and c) Be.

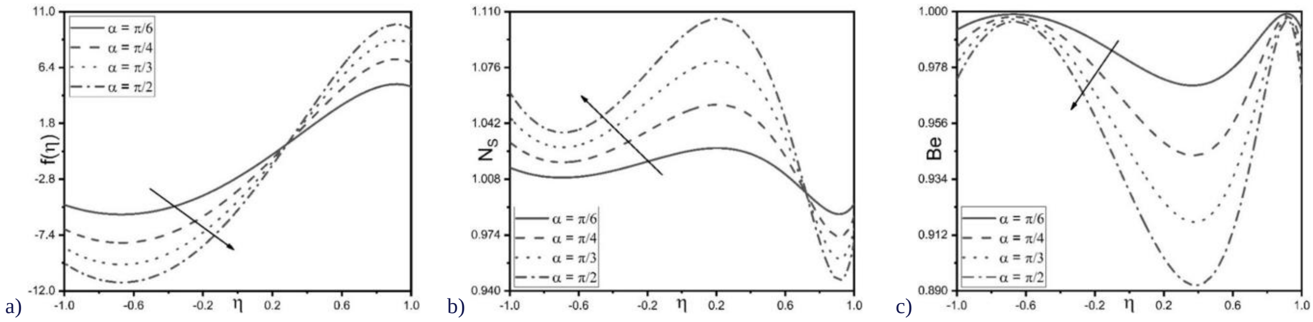

Fig. 3. Impacts of α on: a) f, b) N_S and c) Be.

Figure 4 presents the effects of R_{sc} on f, N_S and Be. As the suction parameter is enhanced, the fluid velocity depletes throughout the channel except near the upper plate. Whereas, the injection parameter increases, the fluid velocity increases throughout the channel except near the upper plate. In the middle of the channel, both suction and injection parameters enhance the velocity (Fig. 4a). Figure 4b represents that the entropy number increases in the middle of the flow channel. This results in the reverse trend of Bejan number (Fig. 4c), indicating the contribution of fluid friction and mass transfer irreversibilities to the generated entropy throughout the channel.

Figure 5 shows the impacts of J on N_S and Be. Increasing the Joule heating parameter increases the entropy generation and hence, N_S increases (Fig. 5a). It impacts on depletion of Bejan number (Fig. 5b). Hence, the Joule heating parameter contributes to entropy generation from combined heat and mass transfer and fluid friction.

It is clear from Fig. 6a that the enhancement in Ha, enhances the fluid velocity, contradicting the anticipated reduction due to the Lorentz force. Similarly, as Ha increases, an increase in entropy number is observed (Fig. 6b). This results in an enhanced Be (Fig. 6c), which signifies the contribution of mass transfer and fluid friction to the generated entropy.

Figure 7 depicts the impacts of S on f, N_S and Be. It is clear from Fig. 7a that the increasing slip velocity values reduce the nanofluid flow velocity near the upper plate. Whereas, it is seen from Fig. 7b that when S increases, the entropy near the surface of the plates decreases and that in the middle of the flow channel increases. This causes an opposite trend in Be (Fig. 7c) thus implying the dominance of fluid friction and mass transfer irreversibilities.

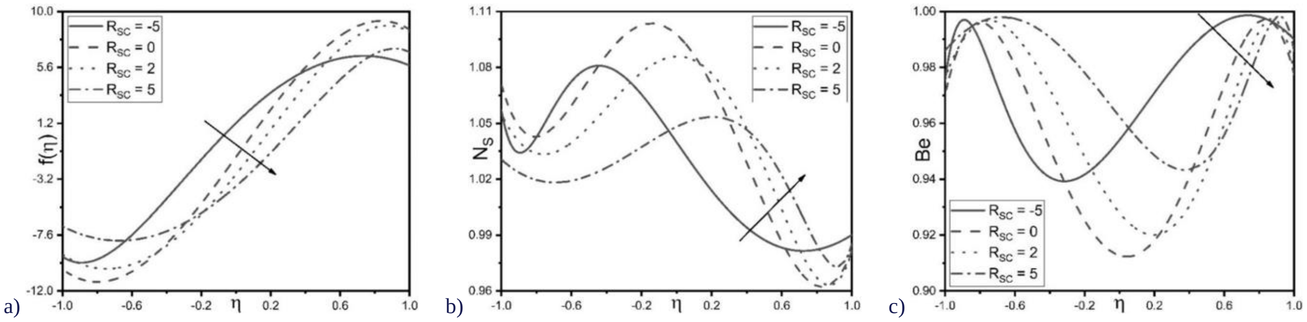

Fig. 4. Impacts of R_{SC} on: a) f, b) N_S and c) Be.

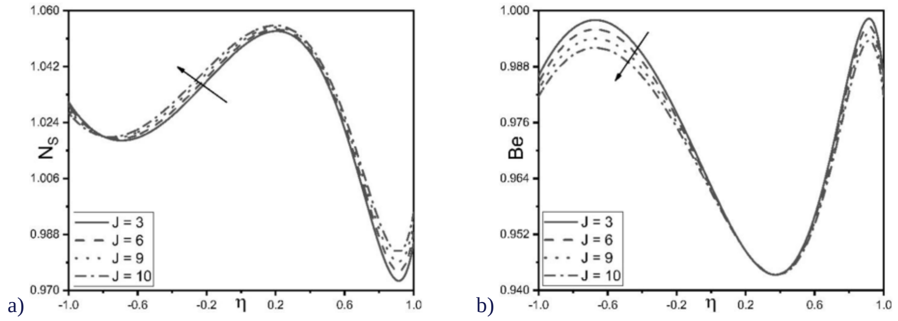

Fig. 5. Impacts of $\boldsymbol{J} \times \mathbf{10^{-5}}$on:(a) N_s and b) Be.

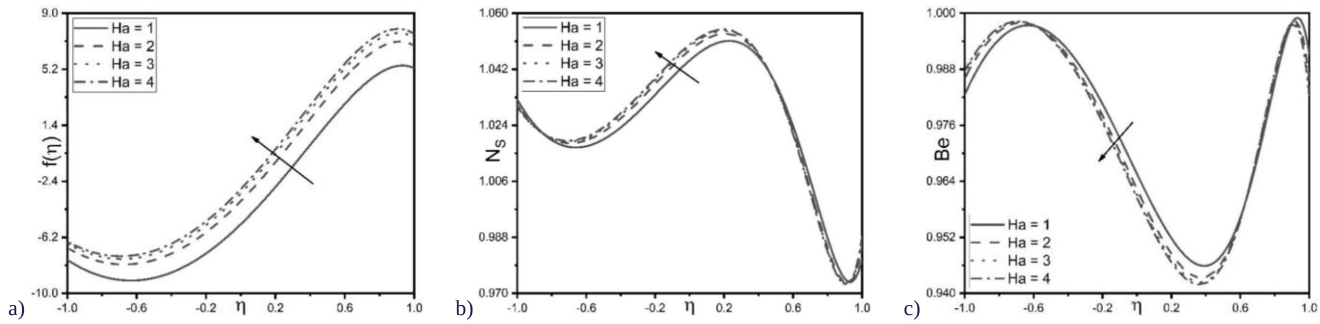

Fig. 6. Impacts of Ha on: a) f, b) N_S and (c) Be.

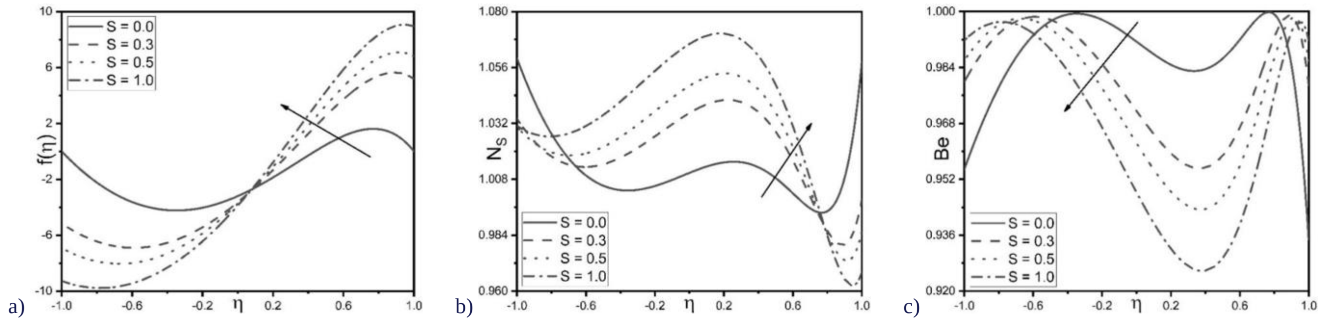

Fig. 7. Impacts of S on: a) f, b) N_S and c) Be.

Table 3 presents the values for Nu, Sh and C_f at the lower plate for different values of the input parameters. The Nusselt number, by definition, is the ratio of heat transfer due to convection to conduction. Clearly, when the parameters R_{sc}, α, Ha and S are increased, Nu and thereby, convective heat transfer quality enhances. While the values of Ha increase, Nu values are supposed to increase, and an enhancement is observed, thus implying the improvement in convective heat transfer quality. Whereas, the injection parameter, N_b, N_t and J reduce the values of Nu. This means, the Joule heating parameter heats up the surface of the channels by conduction and hence a reduction in Nu is observed. Similarly, when Re, N_b, injection parameter and J values are increased, convective mass transfer increases and hence Sh improves, causing an enhancement in convective mass transfer. Likewise, Ha has an improving effect on mass diffusivity, thus resulting in lesser Sh values. Considering the skin friction drag, the parameter N_b, suction parameter, α and J values have a controlling effect on C_f.

Table 3. Nusselt number, Sherwood number and skin friction values, where $J \times 10^{-5}$.

Re	N_b	N_t	R_{SC}	α	J	Ha	S	$-\theta'(1)$	$-\phi'(1)$	$A_7 f'(1)$
100	0.0004	0.0002	5	π/4	3	2	0.5	1.066592	0.966704	-40.024441
200	0.0004	0.0002	5	π/4	3	2	0.5	1.018198	0.990901	-20.920922
300	0.0004	0.0002	5	π/4	3	2	0.5	1.008085	0.995957	-14.06996
400	0.0004	0.0002	5	π/4	3	2	0.5	1.00445	0.997775	-10.586109
300	0.0002	0.0002	5	π/4	3	2	0.5	1.008119	0.991881	-14.021619
300	0.0004	0.0002	5	π/4	3	2	0.5	1.008085	0.995957	-14.06996
300	0.0006	0.0002	5	π/4	3	2	0.5	1.008008	0.997331	-14.086336
300	0.0008	0.0002	5	π/4	3	2	0.5	1.007919	0.99802	-14.09466
300	0.0004	0.0002	5	π/4	3	2	0.5	1.008085	0.995957	-14.06996
300	0.0004	0.0003	5	π/4	3	2	0.5	1.008003	0.993998	-14.046363
300	0.0004	0.0004	5	π/4	3	2	0.5	1.007921	0.992079	-14.022999
300	0.0004	0.0005	5	π/4	3	2	0.5	1.00784	0.990201	-13.999866
300	0.0004	0.0002	-5	π/4	3	2	0.5	1.015474	0.992263	-18.912752
300	0.0004	0.0002	0	π/4	3	2	0.5	1.019284	0.990358	-20.936399
300	0.0004	0.0002	2	π/4	3	2	0.5	1.014996	0.992502	-18.553952
300	0.0004	0.0002	5	π/4	3	2	0.5	1.008085	0.995957	-14.06996
300	0.0004	0.0002	5	π/6	3	2	0.5	1.003926	0.998037	-9.985362
300	0.0004	0.0002	5	π/4	3	2	0.5	1.008085	0.995957	-14.06996
300	0.0004	0.0002	5	π/3	3	2	0.5	1.012178	0.993911	-17.17123
300	0.0004	0.0002	5	π/2	3	2	0.5	1.016207	0.991896	-19.75859
300	0.0004	0.0002	5	π/4	3	2	0.5	1.008085	0.995957	-14.06996
300	0.0004	0.0002	5	π/4	6	2	0.5	1.006763	0.996619	-14.072372
300	0.0004	0.0002	5	π/4	9	2	0.5	1.00544	0.99728	-14.074783
300	0.0004	0.0002	5	π/4	12	2	0.5	1.004118	0.997941	-14.077193
300	0.0004	0.0002	5	π/4	3	1	0.5	1.007139	0.99643	-15.725448
300	0.0004	0.0002	5	π/4	3	2	0.5	1.008085	0.995957	-14.06996
300	0.0004	0.0002	5	π/4	3	3	0.5	1.008418	0.995791	-13.496468
300	0.0004	0.0002	5	π/4	3	4	0.5	1.008588	0.995706	-13.205481
300	0.0004	0.0002	5	π/4	3	2	0	1.006043	0.996978	-27.092764
300	0.0004	0.0002	5	π/4	3	2	0.3	1.0066	0.9967	-17.493855
300	0.0004	0.0002	5	π/4	3	2	0.5	1.008085	0.995957	-14.06996
300	0.0004	0.0002	5	π/4	3	2	1	1.011167	0.994416	-9.433658

6. Conclusions

On examining the flow of water suspended with GO nanoparticles in between two plates aligned with an angle of inclination and including the impacts of Joule heating, we infer the following:

- Velocity is improved by enhancing the Hartman number, Reynolds number and injection parameter values. Hence, the flow is better in the presence of magnetic field.
- Convective heat transfer is improved by the Hartman number, suction parameter, angle of inclination and slip parameter. Therefore, compared to the flow in a horizontal channel where the slip condition is ignored, better thermal performance is achieved with the inclined channel in the presence of a magnetic field and considering slip conditions.
- Brownian motion of the nanoparticles significantly contributes to mass transfer since convective mass transfer is increased by raising values of the Brownian motion parameter, Reynolds number, injection parameter and Joule heating parameter.
- Since Be > 0.9, heat transfer primarily causes the entropy generation, even though the varying parameter values feebly contribute to entropy due to mass transfer and fluid friction.

The problem considered is useful in automobile radiators, heat exchangers, manufacturing polymers and fertilizers, and food processing. The investigation can be further extended by examining the flow of graphene oxide nanofluid in various other geometries and exploring the nanofluid's non-Newtonian behaviour.

References

[1] Buongiorno, J. (2006). Convective transport in nanofluids. *Journal of Heat Transfer*, 128(3), 240–250. doi: 10.1115/1.2150834

[2] Abro, K.A., & Abdon, A. (2022). A computational technique for thermal analysis in coaxial cylinder of one-dimensional flow of fractional Oldroyd-B nanofluid. *International Journal of Ambient Energy*, 43(1), 5357–5365. doi: 10.1080/01430750.2021.1939157

[3] Akram, M., Jamshed, W., Goud, B.S., Pasha, A.A., Sajid, T., Rahman, M.M., Arshad, M., & Weera, W. (2022). Irregular heat source impact on Carreau nanofluid flowing via exponential expanding cylinder: A thermal case study. *Case Studies in Thermal Engineering*, 36, 102171. doi: 10.1016/j.csite.2021.102171

[4] Shah, R.A., Ullah, H., Khan, M.S., & Khan, A. (2021). Parametric analysis of the heat transfer behavior of the nano-particle ionic-liquid flow between concentric cylinders. *Advances in Mechanical Engineering*, 13(6), 16878140211024009. doi: 10.1177/16878140211024009

[5] Javanmard, M., Salmani, H., Taheri, M.H., Askari, N., & Kazemi, M.A. (2021). Heat transfer of a radial, nanofluid water-graphene oxide hydromagnetic flow between coaxial pipes with a variable radius ratio. *Proceedings of the Institution of Mechanical Engineers, Part E: Journal of Process Mechanical Engineering*, 235(1), 124–133. doi: 10.1177/0954408920948194

[6] Masood, S., & Farooq, M. (2021). Influence of thermal stratification and thermal radiation on graphene oxide-Ag/H_2O hybrid nanofluid. *Journal of Thermal Analysis and Calorimetry*, 143, 1361–1370. doi: 10.1007/s10973-020-10227-7

[7] Ramesh, G.K., Shehzad, S.A., & Izadi, M. (2022). Falkner–Skan flow of aqueous magnetite–graphene oxide nanoliquid driven by a wedge. *Chinese Journal of Physics*, 77, 733–746. doi: 10.1016/j.cjph.2021.07.023

[8] Bhattacharyya, A., Sharma, R., Hussain, S.M., Chamkha, A.J., & Mamatha, E. (2022). A numerical and statistical approach to capture the flow characteristics of Maxwell hybrid nanofluid containing copper and graphene nanoparticles. *Chinese Journal of Physics*, 77, 1278–1290. doi: 10.1016/j.cjph.2021.09.015

[9] Lavine, A.S. (1988). Analysis of fully developed opposing mixed convection between inclined parallel plates. *Wärme-und Stoffübertragung*, 23(4), 249–257. doi: 10.1007/BF01807328

[10] Choi, S.U.S., & Eastman, J.A. (1995). *Enhancing thermal conductivity of fluids with nanoparticles*. Argonne National Lab., Argonne, IL (United States), No. ANL/MSD/CP-84938; CONF-951135-29.

[11] Talabi, S.O., & Nwabuko, U. (1993). Numerical solution of natural convective heat transfer in parabolic enclosures. *International Journal of Heat and Mass Transfer*, 36(17), 4275–4281. doi: 10.1016/0017-9310(93)90090-S

[12] Barai, D.P., Bhanvase, B.A., & Sonawane, S.H. (2020). A review on graphene derivatives-based nanofluids: Investigation on properties and heat transfer characteristics. *Industrial and Engineering Chemistry Research*, 59(22), 10231–10277. doi: 10.1021/acs.iecr.0c00865

[13] Azimi, M., Azimi, A., & Mirzaei, M. (2014). Investigation of the unsteady graphene oxide nanofluid flow between two moving plates. *Journal of Computational and Theoretical Nanoscience*, 11(10), 2104–2108. doi: 10.1166/jctn.2014.3612

[14] Gul, T., Ullah, M.Z., Alzahrani, A.K., & Amiri, I.S. (2019). Thermal performance of the graphene oxide nanofluids flow in an upright channel through a permeable medium. *IEEE Access*, 7, 102345–102355. doi: 10.1109/ACCESS.2019.2927787

[15] Shahzad, F., Jamshed, W., Eid, M.R., El Din, S.M., & Banerjee, R. (2023). Mathematical modelling of graphene-oxide/kerosene oil nanofluid via radiative linear extendable surface. *Alexandria Engineering Journal*, 70, 395–410. doi: 10.1016/j.aej.2023.02.034

[16] Nazari, M.A., Ghasempour, R., Ahmadi, M.H., Heydarian, G., & Shafii, M.B. (2018). Experimental investigation of graphene oxide nanofluid on heat transfer enhancement of pulsating heat pipe. *International Communications in Heat and Mass Transfer*, 91, 90–94. doi: 10.1016/j.icheatmasstransfer.2017.12.006

[17] Dehghan, P., Keramat, F., Mofarahi, M., & Lee, C.H. (2023). Computational fluid dynamic analysis of graphene oxide/water nanofluid heat transfer over a double backward-facing microchannel. *Journal of the Taiwan Institute of Chemical Engineers*, 145, 104821. doi: 10.1016/j.jtice.2023.104821

[18] Pashikanti, J., Thota, S., & Priyadharshini, D.R.S. (2024). Effect of viscous dissipation due to magnetohydrodynamic flow in an inclined channel. *Chinese Journal of Physics*, 87, 82–96. doi: 10.1016/j.cjph.2023.11.015

[19] Javanmard, M., Taheri, M.H., Abbasi, M., & Ebrahimi, S.M. (2018). Heat transfer analysis of hydromagnetic water–graphene oxide nanofluid flow in the channel with asymmetric forced convection on walls. *Chemical Engineering Research and Design*, 136, 816–824. doi: 10.1016/j.cherd.2018.06.041

[20] Hafeez, M., Hashim, & Khan, M. (2020). Jeffrey–Hamel flow of hybrid nanofluids in convergent and divergent channels with heat transfer characteristics. *Applied Nanoscience*, 10, 5459–5468. doi: 10.1007/s13204-020-01427-6

[21] Raza, A., Khan, S.U., Khan, M.I., Farid, S., Muhammad, T., Khan, M.I., & Galal, A.M. (2021). Fractional order simulations for the thermal determination of graphene oxide (GO) and molybdenum disulphide (MoS_2) nanoparticles with slip effects. *Case Studies in Thermal Engineering*, 28, 101453. doi: 10.1016/j.csite.2021.101453

[22] Pavithra, K.M., Hanumagowda, B.N., Varma, S.V.K., Ahammad, N.A., Raju, C.S.K., & Noeiaghdam, S. (2023). The impacts of shape factors in a chemically reacting two-passage vertical channel filled with kerosene-based graphene oxide and MoS2 mixture in a porous medium. *Results in Engineering*, 18, 101050. doi: 10.1016/j.rineng.2021.101050

[23] Akram, S., Athar, M., Saeed, K., Razia, A., Muhammad, T., & Hussain, A. (2023). Hybrid double-diffusivity convection and induced magnetic field effects on peristaltic waves of Oldroyd 4-constant nanofluids in non-uniform channel. *Alexandria Engineering Journal*, 65, 785–796. doi: 10.1016/j.aej.2022.10.039

[24] Nazeer, M. (2023). Multiphase flow development in gravitational and magnetic fields. *Waves in Random and Complex Media*, 1−15. doi: 10.1080/17455030.2023.2193853

[25] Yasin, M., Hina, S., & Naz, R. (2023). Influence of inclined magnetic field on peristaltic flow of Ag–Cu/blood hybrid nanofluid in the presence of homogeneous–heterogeneous reactions with slip condition. *Arabian Journal for Science and Engineering*, 48(1), 31–46. doi: 10.1007/s13369-022-06942-y

[26] Srinivasacharya, D., & Bindu, K.H. (2015). Entropy generation in a micropolar fluid flow through an inclined channel with slip and convective boundary conditions. *Energy*, 91, 72–83. doi: 10.1016/j.energy.2015.08.014

[27] Khan, M.N., Ullah, N., & Nadeem, S. (2021). Transient flow of Maxwell nanofluid over a shrinking surface: Numerical solutions and stability analysis. *Surfaces and Interfaces*, 22, 100829. doi: 10.1016/j.surfin.2020.100829

[28] Khan, M.N., & Nadeem, S. (2020). Theoretical treatment of bio-convective Maxwell nanofluid over an exponentially stretching sheet. *Canadian Journal of Physics*, 98(8), 732–741. doi: 10.1139/cjp-2019-0380

[29] Khan, M.N., & Nadeem, S. (2021). A comparative study between linear and exponential stretching sheet with double stratification of a rotating Maxwell nanofluid flow. *Surfaces and Interfaces*, 22, 100886. doi: 10.1016/j.surfin.2020.100886

[30] Nadeem, S., Khan, M.N., Muhammad, N., & Ahmad, S. (2019). Mathematical analysis of bio-convective micropolar nanofluid. *Journal of Computational Design and Engineering*, 6(3), 233−242. doi: 10.1016/j.jcde.2019.04.001

[31] Khan, M.N., Nadeem, S., & Muhammad, N. (2020). Micropolar fluid flow with temperature-dependent transport properties. *Heat Transfer*, 49(4), 2375–2389. doi: 10.1002/htj.21726

[32] Nadeem, S., Khan, M.N., & Abbas, N. (2020). Transportation of slip effects on nanomaterial micropolar fluid flow over exponentially stretching. *Alexandria Engineering Journal*, 59(5), 3443−3450. doi: 10.1016/j.aej.2020.05.024

[33] Ahmad, S., Nadeem, S., Muhammad, N., & Khan, M.N. (2021). Cattaneo–Christov heat flux model for stagnation point flow of micropolar nanofluid toward a nonlinear stretching surface with slip effects. *Journal of Thermal Analysis and Calorimetry*, 143, 1187–1199. doi: 10.1007/s10973-020-09504-2

[34] Khan, M.N., Nadeem, S., Ullah, N., & Saleem, A. (2020). Theoretical treatment of radiative Oldroyd-B nanofluid with microorganism pass an exponentially stretching sheet. *Surfaces and Interfaces*, 21, 100686. doi: 10.1016/j.surfin.2020.100686

[35] Gul, T., Ullah, M.Z., Alzahrani, A.K., & Amiri, I.S. (2019). Thermal performance of the graphene oxide nanofluids flow in an upright channel through a permeable medium. *IEEE Access*, 7, 102345–102355. doi: 10.1109/access.2019.2927787

[36] Elsaid, K., Abdelkareem, M.A., Maghrabie, H.M., Sayed, E.T., Wilberforce, T., Baroutaji, A., & Olabi, A.G. (2021). Thermophysical properties of graphene-based nanofluids. *International Journal of Thermofluids*, 10, 100073. doi: 10.1016/j.ijft.2021.100073

[37] Al-Sankoor, K., Al-Gayyim, H., Al-Musaedi, S., Asadi, Z., & Ganji, D.D. (2021). Analytically investigating of heat transfer parameters with presence of graphene oxide nanoparticles in Williamson-magnetic fluid by AGM and HPM methods. *Case Studies in Thermal Engineering*, 27, 101236. doi: 10.1016/j.csite.2021.101236

[38] Lide, D.R. (Ed.). (2004). *CRC handbook of chemistry and physics*. (Vol. 85). CRC Press.

[39] Ghadikolaei, S.S., Hosseinzadeh, K.H., Hatami, M., Ganji, D.D., & Armin, M. (2018). Investigation for squeezing flow of ethylene glycol ($C_2H_6O_2$) carbon nanotubes (CNTs) in rotating stretching channel with nonlinear thermal radiation. *Journal of Molecular Liquids*, 263, 10–21. doi: 10.1016/j.molliq.2018.04.141

[40] Chu, Y.M., Nisar, K.S., Khan, U., Kasmaei, H.D., Malaver, M., Zaib, A., & Khan, I. (2020). Mixed convection in MHD water-based molybdenum disulfide-graphene oxide hybrid nanofluid through an upright cylinder with shape factor. *Water*, 12(6), 1723. doi: 10.3390/w12061723

[41] Bejan, A. (1996). Entropy generation minimization: The new thermodynamics of finite-size devices and finite-time processes. *Journal of Applied Physics*, 79(3), 1191–1218. doi: 10.1063/1.362674

[42] Bejan, A., & Kestin, J. (1983). Entropy generation through heat and fluid flow. Journal of Applied Mechanics, 50(2), 475-475. doi: 10.1115/1.3167072

[43] Paoletti, S., Rispoli, F., & Sciubba, E. (1989). Calculation of exergetic losses in compact heat exchanger passages. *ASME, Advanced Energy Systems*, 10(2), 21–29.

[44] Bellman, R.E. (1965). *Quasilinearization and nonlinear boundary-value problems*. (Vol. 3). American Elsevier Publishing Company.

[45] Canuto, C., Hussaini, M.Y., Quarteroni, A., & Zang, T.A. (2007). *Spectral methods: fundamentals in single domains*. Springer Science & Business Media.

[46] Malashetty, M.S., Umavathi, J.C., & Prathap Kumar, J. (2001). Convective magnetohydrodynamic two fluid flow and heat transfer in an inclined channel. *Heat and Mass transfer*, 37(2−3), 259−264. doi: 10.1007/s002310000134

[47] Behseresht, A., Noghrehabadi, A., & Ghalambaz, M. (2014). Natural-convection heat and mass transfer from a vertical cone in porous media filled with nanofluids using the practical ranges of nanofluids thermo-physical properties. *Chemical Engineering Research and Design*, 92(3), 447–452. doi: 10.1016/j.cherd.2013.08.028

[48] Makinde, O.D., & Eegunjobi, A.S. (2013). Effects of convective heating on entropy generation rate in a channel with permeable walls. *Entropy*, 15(1), 220–233. doi: 10.3390/e15010220